Heliyon 10 (2024) e27134

Contents lists available at ScienceDirect

Heliyon

journal homepage: www.cell.com/heliyon

Research article

Single crystal synthesis and physical property of $Ba_8Cu_{1.0}Ni_{2.5}Ga_{10}Si_{33.5}$ clathrate

Pooja Rawat [a,b], Aanchal Sethi [c], Jin Hee Kim [a], Jong Soo Rhyee [a,*]

[a] Department of Applied Physics and Institute of Natural Sciences, Integrated Education Institute for Frontier Science and Technology (BK21 Four), Kyung Hee University, Yong-in 17104, Republic of Korea
[b] Department of Chemistry, Biochemistry and Forensic Science, Amity School of Applied Sciences, Amity University Haryana, Gurugram, Haryana 122413, India
[c] Department of Chemistry, Swami Shraddhanand College, University of Delhi, Delhi-110036, India

ARTICLE INFO

Keywords:
Single crystal
Inorganic clathrate
Ferromagnetic
Metallic
Heat capacity

ABSTRACT

This study reports the synthesis of type-I $Ba_8CuNi_{2.5}Ga_{10}Si_{33.5}$ clathrate as a single crystal by the flux method and physical properties investigations such as structural, chemical, magnetic, and thermal properties. Structural refinements indicate Ba atoms are situated at 2a and 6d positions with mixed occupancy across framework sites. Raman spectroscopy assessed host-guest interactions, while the compound's morphology and composition were investigated by the scanning electron microscopy (SEM), energy dispersive X-ray spectroscopy (EDS), and X-ray photoelectron spectroscopy (XPS) analyses. Magnetic properties revealed ferromagnetic interactions characterized by a positive Weiss constant and weak ferromagnetic hysteresis. The compound's metallic nature is evidenced by increased resistivity with temperature. The Sommerfeld coefficient, estimated at 12.59 mJ mol^{-1} K^{-2} from heat capacity data, alongside a pronounced peak around 15 K in the C_p/T^3 vs T plot, suggests an Einstein contribution in heat capacity.

1. Introduction

The quest for materials with exceptional properties has driven researchers to explore unconventional crystalline structures, leading to the discovery of single crystal inorganic clathrates [1–4]. Clathrate, a three dimensional structured polyhedral represents an interesting class of crystalline host-guest compounds with Na_8Si_{46} being the first member of the inorganic clathrate family [5]. The three-dimensional framework structure consists of six tetrakaidecahedrons and two dodecahedrons units forming a cage for the insertion of metal atom. Typically, this anionic framework structure is made up of group 13 or 14 element while the group 1 or 2 elements act as guest atoms. Of these, the group 14 clathrate type I materials have been studied extensively [6–8].

A careful manipulation of the guest atoms within the silicon cages tailors the electronic and thermal properties of these framework structures thereby, opening up new avenues for novel electronic and optoelectronic devices [9,10]. One intriguing facet to studying inorganic clathrates involves exploring the impact of cation occupancy and the influence of intermolecular interaction as well as unique structural characteristics, in precisely adjusting their physical properties.

In single crystal inorganic clathrates, the host lattice and guest molecules or atoms interact in a manner that creates voids or channels within the crystal structure [3,4]. These voids can accommodate guest species, which are often of a different size or chemical

* Corresponding author.
E-mail address: jsrhyee@khu.ac.kr (J.S. Rhyee).

https://doi.org/10.1016/j.heliyon.2024.e27134
Received 22 December 2023; Received in revised form 16 February 2024; Accepted 24 February 2024
Available online 27 February 2024

nature compared to the host atoms or molecules. The resulting clathrate compounds exhibit a range of remarkable properties, including low thermal conductivity, intriguing electronic behavior, and even the potential for thermoelectric applications [9–11]. The unique host-guest architecture of single crystal inorganic clathrates arises from a delicate interplay of factors, including the sizes, shapes, and chemical affinities of the host and guest species. This intricate dance of interactions forms the basis for their remarkable properties, making them appealing subjects for research in diverse fields. As researchers delve into their synthesis and characterization, a wealth of possibilities emerges, spanning from fundamental physics to cutting-edge technological applications.

Different methods are employed in the synthesis of clathrates, primarily determined by the chemical characteristics of the elements involved in forming the clathrate lattice. The majority of intermetallic clathrates incorporate one of the Group 14 elements (Si, Ge, Sn), and the choice of synthesis method depends on their reactivity [8,9]. Silicon, due to its high melting point, exhibits lower reactivity in high-temperature reactions used for clathrate production. A common approach for creating silicon-based clathrates involves heating the relevant elements above their melting points and subsequent annealing. This synthetic path is also conducive to producing ternary or quaternary clathrates [5,9]. As an example, Beekman et al. achieved the crystal growth of $Na_{24}Si_{136}$ clathrate by heating Na_4Si_4 under 100 MPa uniaxial pressure and 823–973 K temperatures range using spark plasma sintering (SPS) system [12]. Other methods, such as preceding arc melting and annealing, have been utilized for clathrate synthesis, as demonstrated in the case of $K_7B_7Si_{39}$ [13].

The magnetic properties of single crystal clathrates can vary significantly depending on the specific composition and arrangement of guest atoms within the cage-like structure [14,15]. Unlike traditional magnetic materials, clathrates do not inherently possess magnetic moments in their host framework (e.g., silicon or germanium cages). Instead, the magnetic properties are primarily attributed to the guest atoms that are encapsulated within the cages [14]. The interaction between the magnetic moments of guest atoms and their surroundings plays a crucial role in prompting the magnetic properties. Extensive research on the thermoelectric properties of type I clathrates have been carried out and a plethora of literature reports are available; but a similar investigation about the magnetic properties of these framework structures is quite limited. This paper delves into the current state-of-the-art techniques utilized in the growth of high-quality single crystal clathrates and the fundamental principles governing their crystallographic arrangements. A careful structural investigation along with detailed magnetic properties have been reported in this paper.

2. Experimental section

2.1. Synthetic procedure

The single crystal clathrate synthesized by the flux reaction by using high purity Ba, Cu, Ni, Si and Ga elements in a stoichiometric ratio of $Ba_8Cu_{1.0}Ni_{2.5}Ga_{10}Si_{33.5}$. Ga acting as flux was taken in slight excess, later the residual flux was washed with dilute acid. The respective weights (as per the required composition) of all these elements were heated to 1000 °C for 12 h followed by a slow cooling in an electric box furnace. The whole procedure for the single crystal synthesis represented in Fig. 1.

2.2. Characterization

Powder X-ray diffraction (PXRD) of the grounded single crystal sample were measured from $2\theta = 10–70^\circ$ on Bruker employing Cu k_α radiation for phase and structural investigation. Initially, the PXRD patterns were fitted by Le Bail method followed by Rietveld refinements (GSAS + EXPGUI) program [16]. The set of refined parameters included lattice parameter, background, scale factor, profile function coefficients, atomic positions, occupancies, thermal parameters. The atoms present on the identical sites were constrained to have same positional and thermal parameters. Raman analysis was performed using Renishaw with 513 nm laser source.

The morphology and composition analysis were carried out by SEM (MERLIN, Carl Zeiss, Germany) and EDX (Oxford instrument, England). The oxidation state of the respective elements was measured by XPS analysis using K-Alpha (Thermo Fisher Scientific, U.S. A.). Magnetic and specific heat measurements were conducted using the Physical Property Measurement System (PPMS Dynacool 14 T) by Quantum Design, USA, at temperatures below 300 K. Additionally, a vibrating sample magnetometer (VSM) option was

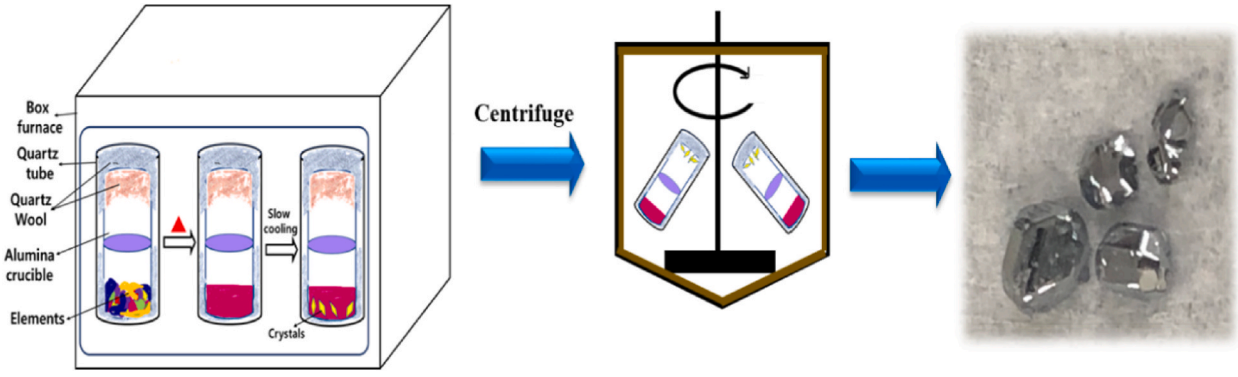

Fig. 1. Schematic representation of $Ba_8Cu_{1.0}Ni_{2.5}Ga_{10}Si_{33.5}$ single crystal synthesis.

employed. Electrical resistivity measurements were performed using the 4-point probe contact method, utilizing a cryogen-free Physical Property Measurement System (PPMS Dynacool 14T) from Quantum Design, USA, without applying a magnetic field. The Hall coefficient was determined using the van der Pauw technique with a current of 10 mA, employing the PPMS system.

3. Results and discussion

The X-ray diffraction (XRD) pattern of pulverized $Ba_8Cu_{1.00}Ni_{2.5}Ga_{10}Si_{33.5}$ single crystal is consistent with type-I clathrate phase. The crystal structure was analyzed based on the model of type-I inorganic clathrate and the crystallographic data was deduced by the Rietveld refinement with the XRD data at room temperature. The refinement of $Ba_8Cu_{1.0}Ni_{2.5}Ga_{10}Si_{33.5}$ clathrate was performed using *Pm-3n* (no. 223) space group with lattice parameter $a = 10.54545$ (9) Å shown as Fig. 2.

The structural refinement resulted in a framework structure consisting of two cages formed by Si, Ga, Ni/Cu encapsulating Ba as the guest atoms. The first cage consists of 20 atoms forming a small dodecahedra whereas the second cage consists of 24 atoms forming the tetrakaidecahedra. In essence, the framework is formed by these face sharing polyhedra's with guest atoms located in the cages. Both these cages i.e; pentagonal dodecahedral and tetrakaidecahedral are shown in Fig. 3.

The heavier atoms i.e; Ba are situated at *2a* and *6d* positions while other atoms (Si, Ga, Cu, Ni) are forming the framework structure. Based on literature reports, the site preference of Ga in the structure has a significant effect on the structure stability along with the magnetic and thermoelectric properties. The trivalent atom usually gets shared among all the three framework sites in such a way that decrease the energetically unfavorable bonding among them. Thus, the site preference (*6c* > *24k* > *16i*) of Ga here is quite similar to other type-I clathrates [9]. Cu prefers to occupy the *6c* site whereas Ni is located at *24k* site, thus both these sites show mixed occupancy. The transition metals generally prefer to occupy the *6c* site thus; a close competition between Cu and Ni is present [17,18]. Also, the *6c* site has the lowest Mulliken population therefore, the element with less electronegativity occupies this site [19]. Cu and Ni have comparable electronegativity values ($\chi_{Cu} = 1.90$ and $\chi_{Ni} = 1.91$) but Cu has a slightly lower value and thus further justifying the *6c* site preference for Cu. Thus, Cu prefers to occupy the *6c* site whereas Ni is located at *24k* site, and both these sites show mixed occupancy. The atomic parameters and occupancies were repeatedly refined until a good agreement between the experimental and structural model was obtained and the refined composition was $Ba_{8.0}Ga_{11.52}Cu_{1.14}Ni_{2.16}Si_{31.18}$ and is very close to the starting nominal stoichiometry. Atomic positions, site occupancies and isotropic thermal parameters are listed in Table 1 and the bond distance and bond length reported as Table 2.

The chemical formula calculated from refined occupancies was found to be ($Ba_{8.0}Ga_{11.52}Cu_{1.14}Ni_{2.16}Si_{31.18}$) and is in considerable agreement with the results from EDS and XPS measurements (discussed later).

Fig. 4 displays the Raman spectrum of the sample, revealing a distinct prominent peak at approximately 514 cm^{-1}, along with a broad spectral envelope spanning the range of 250–400 cm^{-1}, which could possibly result from a combination of partially resolved peaks. A comparable spectrum was observed in the case of $Ba_{7.5}Al_{13}Si_{29}$ and $Eu_{0.27}Ba_{7.22}Al_{13}Si_{29}$ samples, where a robust band at 516 cm^{-1} and a wide peak ranging from about 200 to 400 cm^{-1} were previously reported [20].

Shimizu et al. reported that the highest frequency band can be used as an efficient tool to analyze the extent of interaction of the guest atoms with the framework structure [21,22]. The highest frequency peak in the present case is attributed to the Ga–Si/TM framework vibrations. The strong band indicates a weak host guest interaction compared to Ba_8Si_{46} and a similar behavior was also observed in $Ba_8Ga_{16}Si_{30}$ inorganic clathrate [22]. The poorly separated bands at lower frequency are due to the rattling guest atoms [22].

The chemical homogeneity of the sample was analyzed by the elemental mapping of Ba, Ga, Si, Ni and Cu as shown in Fig. 5. All the samples are uniformly distributed thereby depicting the homogeneous nature of the prepared sample. From the quantitative EDS

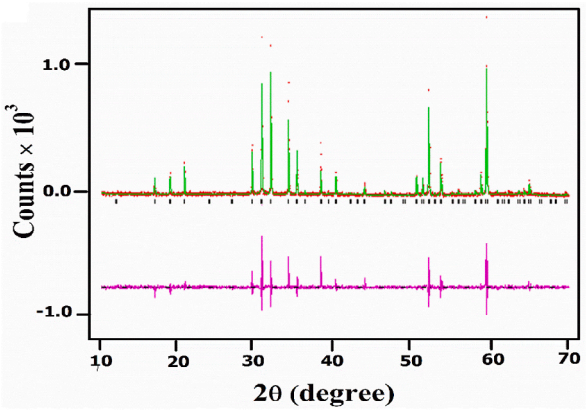

Fig. 2. Structure refinement of the $Ba_8Cu_{1.0}Ni_{2.5}Ga_{10}Si_{33.5}$ single crystal clathrate. The Bragg positions correspond to cubic (*Pm-3n*; black color) structure. The red color pattern represents the experimental data while the green color plot depicts the calculate data. The pink color line shows the extent of fitting between the experimental and the calculated pattern and the vertical black tick marks correspond to the Bragg reflections. (For interpretation of the references to color in this figure legend, the reader is referred to the Web version of this article.)

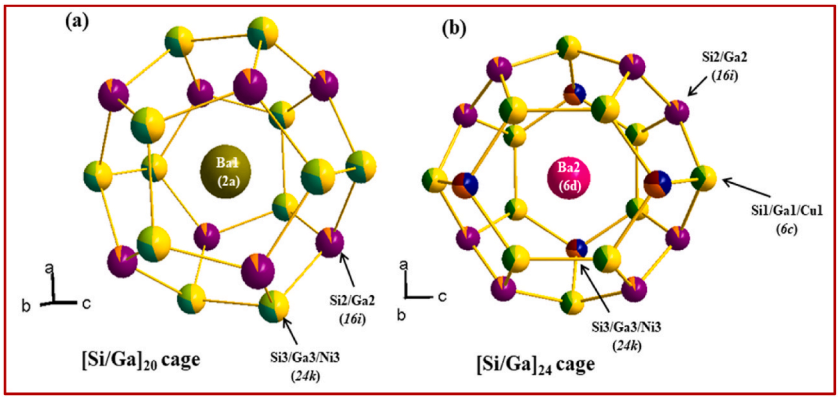

Fig. 3. Ball and stick model representation of $[Si/Ga]_{20}$ (a) and $[Si/Ga]_{24}$ (b) cages of the crystal ($Ba_{8.0}Ga_{11.12}Cu_{1.14}Ni_{2.16}Si_{31.58}$).

Table 1
Crystallographic data for $Ba_8Cu_{1.0}Ni_{2.5}Ga_{10}Si_{33.5}$ single crystal clathrate in space group *Pm-3n* (no. 223), $a = 10.54545(9)$ Å, $V = 1172.723(11)$ Å^3, $\chi^2 = 2.349$, $R_{wp} = 7.11$ %, $R_p = 5.15$ %.

Atoms	*Wyck*	*x*	*y*	*z*	SOF	U(iso) (Å^2)
Ba1	*2a*	0	0	0	1	0.022(3)
Ba2	*6d*	0.25	0.50	0	1	0.027(2)
Si1/Ga1/Cu	*6c*	0.25	0	0.50	0.25/0.56/0.19(4)	0.0090(4)
Si2/Ga2	*16i*	0.18672(3)	0.18672(3)	0.18672(3)	0.91/0.09(6)	0.0087(3)
Si3/Ga3/Ni3	*24k*	0	0.30521(3)	0.1191(3)	0.63/0.28/0.09(3)	0.0093(4)

Table 2
Distance between different Wyckoff sites and bond angles.

	Bond length (Å)	Bond angles (°)
2a-24k	3.45511(1)	24k-16i-24k 109.8275(4)
2a-16i	3.41078(1)	16i-16i-24k 109.1126(1)
16i-16i	2.31161(2)	24k-6c-24k 108.1244(1)
16i-24k	2.43880(5)	16i-24k-6c 105.1995(2)
24k-24k	2.51220(1)	16i-24k-16i 107.0020(1)
6c-24k	2.47499(2)	16i-24k-24k 107.6959(2)
		6c-24k-24k 123.9001(2)

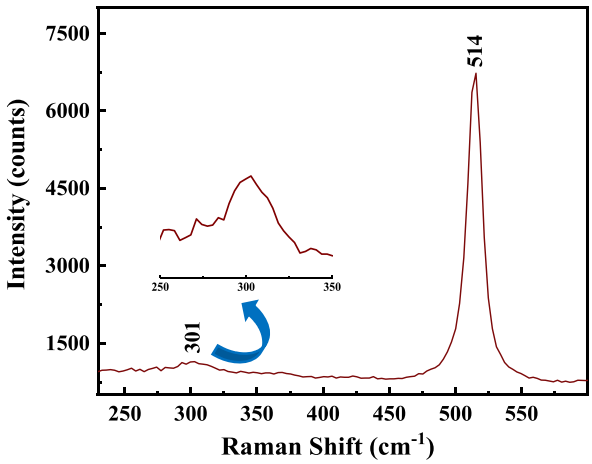

Fig. 4. Raman spectrum of $Ba_8Cu_{1.0}Ni_{2.5}Ga_{10}Si_{33.5}$ single crystal clathrate.

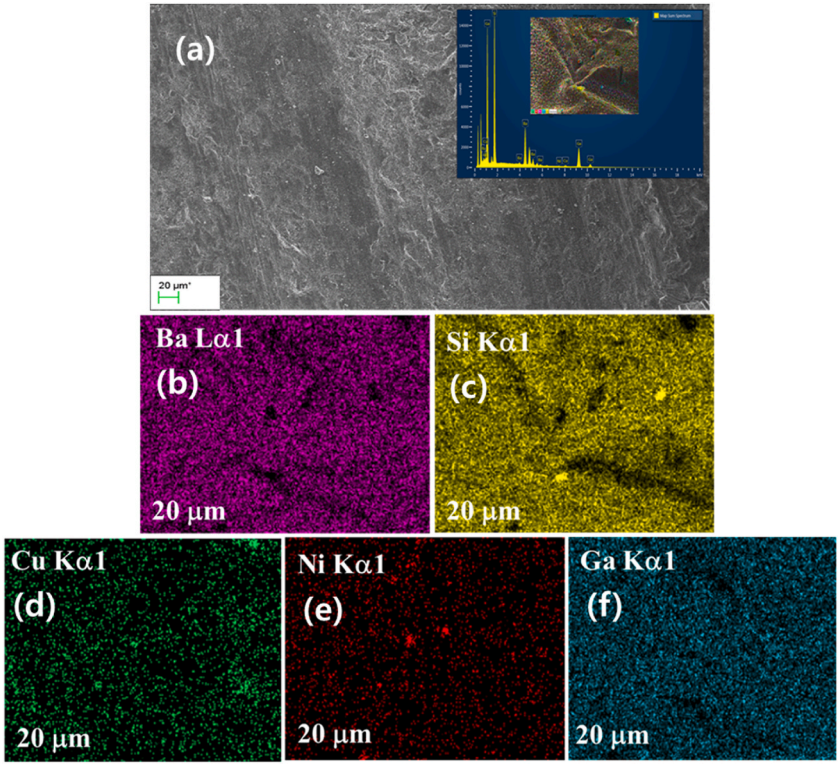

Fig. 5. (a) Scanning electron microscope (SEM) and energy dispersive X-ray spectroscopy (EDS, inset) images. Elemental mapping images of Ba (b), Si (c), Cu (d), Ni (e), and Ga (f) of $Ba_8Cu_{1.0}Ni_{2.5}Ga_{10}Si_{33.5}$ single crystal clathrate.

analysis, the elemental concentrations in a single crystal clathrate composition were calculated to be $Ba_8Cu_{1.0}Ni_{1.9}Ga_{18}Si_{38.8}$. X-ray photoelectron spectroscopy (XPS) studies were performed for the single crystal sample from Fermi to core levels for better understanding the differences in the chemical surface states. It revealed the valence band is mainly constructed by the Ga/Si (3d/2p) wave function and slight contribution from Ba (3d) orbital. In Fig. 6(a), we observed the Ba $3d_{3/2}$ and Ba $3d_{5/2}$ peaks at binding energies of 93.0 and 90.3 eV, respectively. Simultaneously, in Fig. 6(c), the Si $2p_{3/2}$ peak was detected at 99 eV, corresponding to the Si atoms within the clathrate framework. The pronounced intensity of the Si peaks signifies a robust Si–Si interaction. Notably, due to the interaction between Si and Ba, the binding energy of Si within the clathrate structure is shifted to a lower energy level and exhibits reduced intensity compared to what is observed in diamond cubic Si [23]. Fig. 6(b) shows the Ga 3d core-level spectra with overlapping $Ga3d_{5/2}$ and $Ga3d_{3/2}$ (~19.6 eV) that might be attributed to the small spin-orbit interaction. The peak around 26 eV corresponds to the Ga auger peak [24].

The elemental composition calculated from XPS analysis for the single crystal corresponds to $Ba_{8.035}Cu_{1.19}Ni_{1.82}Ga_{10.28}Si_{35.68}$ which is in considerable agreement with the structural refinement and EDS results discussed earlier.

The magnetic susceptibility measurement with temperature dependence is shown in Fig. 7(a) at an applied field of 1 T. The magnetic curve clearly indicates a ferromagnetic to paramagnetic transition with increase in temperature. The variation in magnetic susceptibility was also measured under different magnetic field ($0.1T \leq H \leq 5T$) (inset of Fig. 7 (a)). In the high-temperature range ($T > 50K$), the reciprocal of magnetic susceptibility was fitted using the Curie-Weiss law, expressed as $\chi = C/(T - \theta)$, where θ represents the Weiss constant, C denotes the Curie constant, and T signifies temperature (as depicted in Fig. 7(b)) [25].

The effective magnetic moment was estimated to be 3.87 μ_B and a positive Weiss constant of 11.32 K points towards overall ferromagnetic interactions in the sample. Usually, Cu atoms are non-magnetic in such framework structures but the high value of magnetic moment indicates the contribution from Cu^{2+} also [26,27]. A similar magnetic behavior was reported in type-I Ge clathrate compound, $Ba_8Cu_5Ge_{40}$ wherein; the high value of magnetic moment was ascribed to the composite clusters formed by the neighbouring atoms, centered around Cu atoms. The competing internal interactions in the framework in these clusters lead to such peculiar magnetic behavior. The experimental magnetic moment is a bit lower than the theoretical magnetic moment (4.14 μ_B calculated by the contribution of Ni^{2+} and Cu^{2+}). A slightly lower experimental value may be attributed to magnetic inhomogeneity and further competing interactions occurring between the magnetically active ions.

Fig. 8 shows the isothermal magnetization measuring from −1 to 1 T at different temperature ranging from 2 K to 100 K, as indicated. A hysteresis loop observed at 2K temperature corresponds to the weak ferromagnetic coupling in the sample. The magnetization curve at high temperature ($T > 20$ K) is linear with the applied field indicating a paramagnetic state.

The temperature dependence electrical resistivity of $Ba_8Cu_{1.0}Ni_{2.5}Ga_{10}Si_{33.5}$ single crystal clathrate normalized to the value at 300

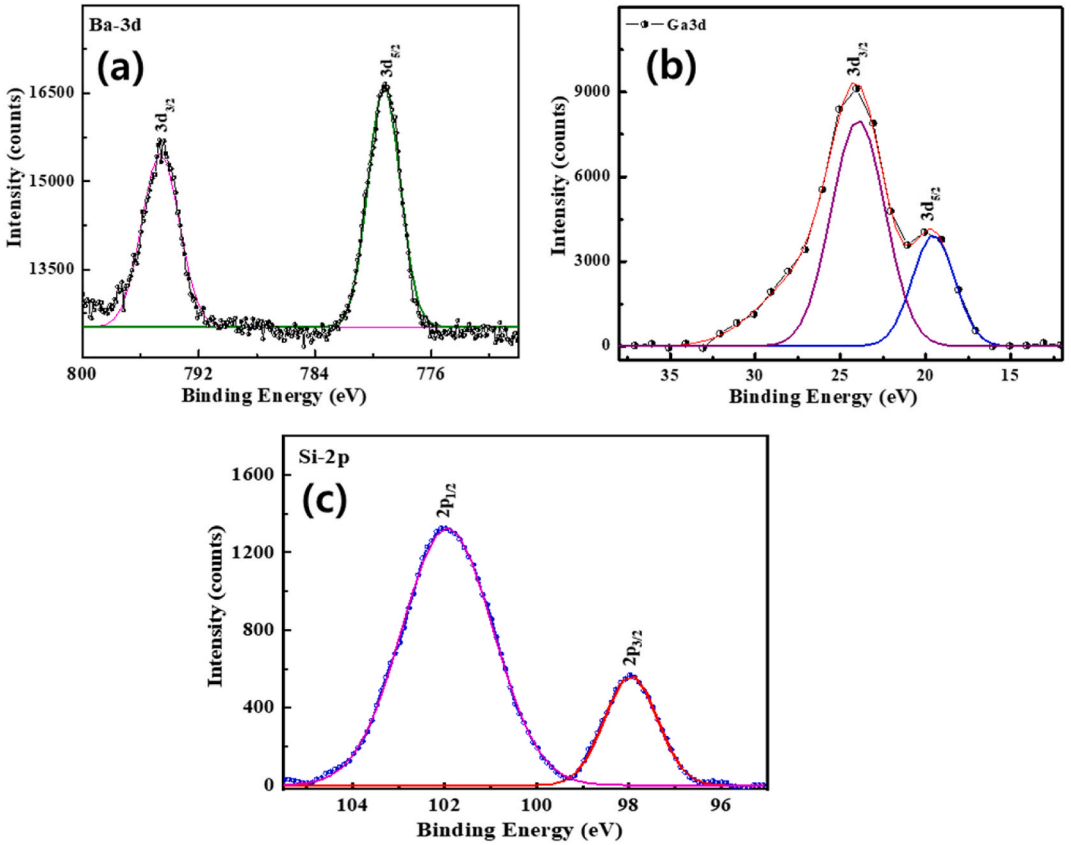

Fig. 6. Core level X-ray photoelectron spectroscopy (XPS) spectra of Ba 3d (a), Ga 3d (b), and Si 2p (c) for $Ba_8Cu_{1.0}Ni_{2.5}Ga_{10}Si_{33.5}$ single crystal clathrate.

K (ρ_T/ρ_{300K}) is plotted as Fig. 9. A linear increase in resistivity with increase in temperature shows a metallic behavior with positive value (ρ_T/ρ_{300K}). Theoretical predictions suggested the involvement of electrons and holes together in the electrical conduction of this material. This behavior can be explained by considering that mobility, along with the concentration of holes and electrons, is closely linked to the nickel content and the intricate details of the material's band structure [28]. This observed metallic behavior aligns with the concept of holes as free charge carriers, as indicated by electron counting. The Hall resistance measured for the single crystal using van der Pauw technique. The Hall resistivity at room temperature was measured to be 1.669 μΩ-cm. The Hall coefficient, typically denoted as R_H, can be expressed generally by the following relationship: $R_H = 1/(ne)$, where 'n' represents the carrier concentration, and 'e' corresponds to the elementary charge. The value of Hall coefficient was calculated to be 0.0347 $cm^3\ C^{-1}$ at room temperature. The carrier concentration and carrier mobility calculated using the hall measurement data for the $Ba_8Cu_{1.0}Ni_{2.5}Ga_{10}Si_{33.5}$ single crystal clathrate comes to be 1.8×10^{20} cm^{-3} and 87.7 $cm^2\ V^{-1}\ s^{-1}$, respectively.

The specific heat of $Ba_8Cu_{1.0}Ni_{2.5}Ga_{10}Si_{33.5}$ single crystal clathrate is shown as Fig. 10 (a). For the analysis, it can be considered as a combination of both phononic and electronic contributions. The electronic specific heat, denoted as C_{el}, was determined to be 0.0125 J $mol^{-1}\ K^{-1}$. It is hypothesized that the significant contribution to heat capacity in type-I clathrates primarily arises from the rattling motion of guest atoms within the larger 24-vertex cages. A distinct maximum near 12.1 K (Fig. 10 (a)) can be attributed to Einstein vibration modes of the guest atoms [28]. At higher temperatures (50–300 K), together with the Einstein components of the heat capacity, the Debye component $C_D(T)$ begins to play an increasingly important role. This estimation was derived from a linear fit of C_p/T vs. T^2 for temperatures below 5 K, employing the Debye model ($C_p = \gamma T + \beta T^3$, where γ represents the Sommerfeld coefficient, and β corresponds to the lattice contribution to the heat capacity), as illustrated in Fig. 10(b) [29,30]. The Sommerfeld coefficient value is found to be 12.59 mJ $mol^{-1}\ K^{-2}$ and it is quite lower as compared to the reported value for $Ba_8Ni_{3.1}Si_{42.9}$ clathrate ($\gamma = 28.8$ mJ $mol^{-1}\ K^{-2}$) [30]. The lower Sommerfeld coefficient value can correspond to the weak ferromagnetism, and disordering behavior in the single crystal. The low-temperature Einstein contribution indicates the existence of localized guest atoms vibration within the cages, as in to conventional tetrel clathrates [31,32]. This contribution at low temperatures can be directly derived from the specific heat data. A graphical representation of C_p/T^3 vs. T, in the inset of Fig. 10(b), displays a prominent peak, typically occurring at approximately 15 K.

Additional investigation involving neutron diffraction, detailed magnetic measurements coupled with electronic calculations will help in further understanding of the peculiar framework structure.

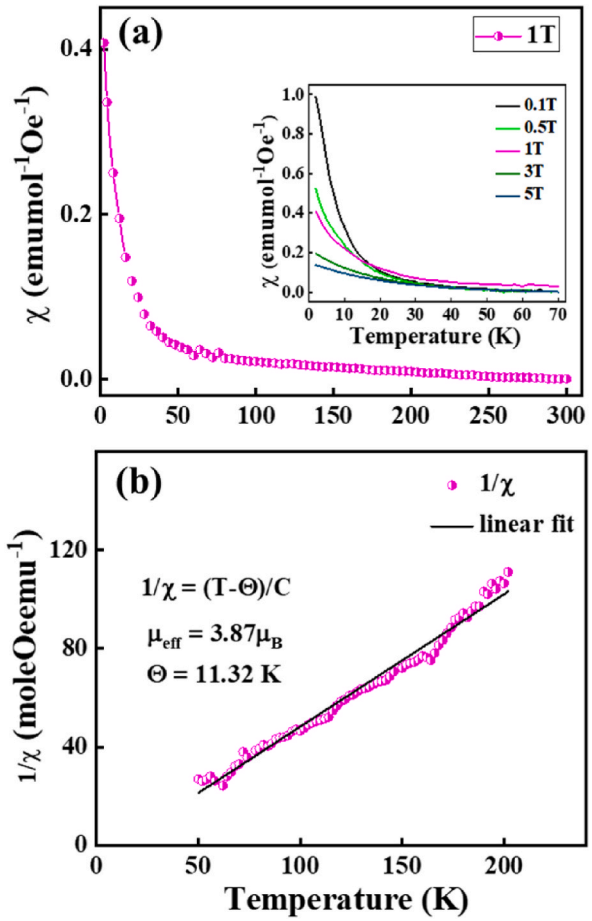

Fig. 7. (a) Magnetic susceptibility variation with temperature of $Ba_8Cu_{1\cdot0}Ni_{2.5}Ga_{10}Si_{33.5}$ single crystal clathrate in an external field of 1 T and (b) The inverse magnetic susceptibility showing Curie-Weiss fit in high temperature region. Inset of (a) shows the temperature-dependent magnetic susceptibility at different magnetic fields, as indicated.

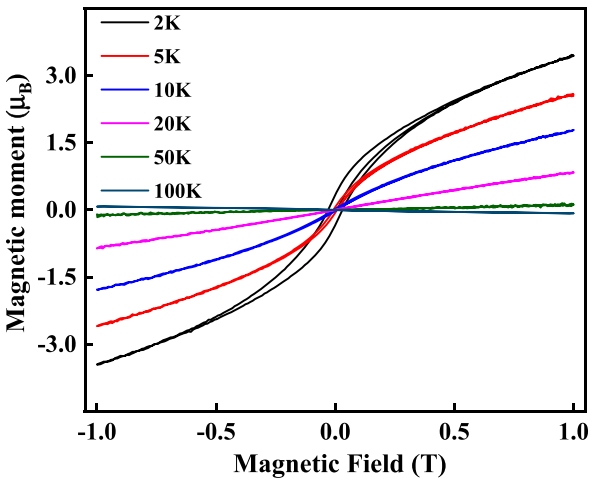

Fig. 8. Variation in Isothermal magnetization with field at different temperatures, as indicated (2, 5, 10, 20, 50, 100 K) for $Ba_8Cu_{1\cdot00}Ni_{2.5}Ga_{10}Si_{33.5}$ single crystal clathrate.

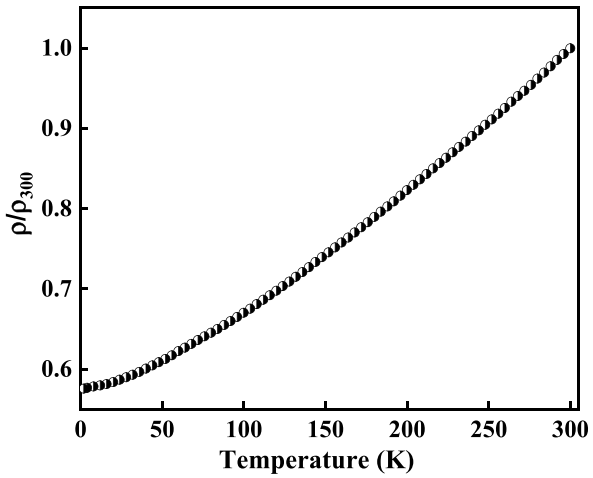

Fig. 9. Temperature dependent electrical resistivity of $Ba_8Cu_{1.0}Ni_{2.5}Ga_{10}Si_{33.5}$ single crystal clathrate.

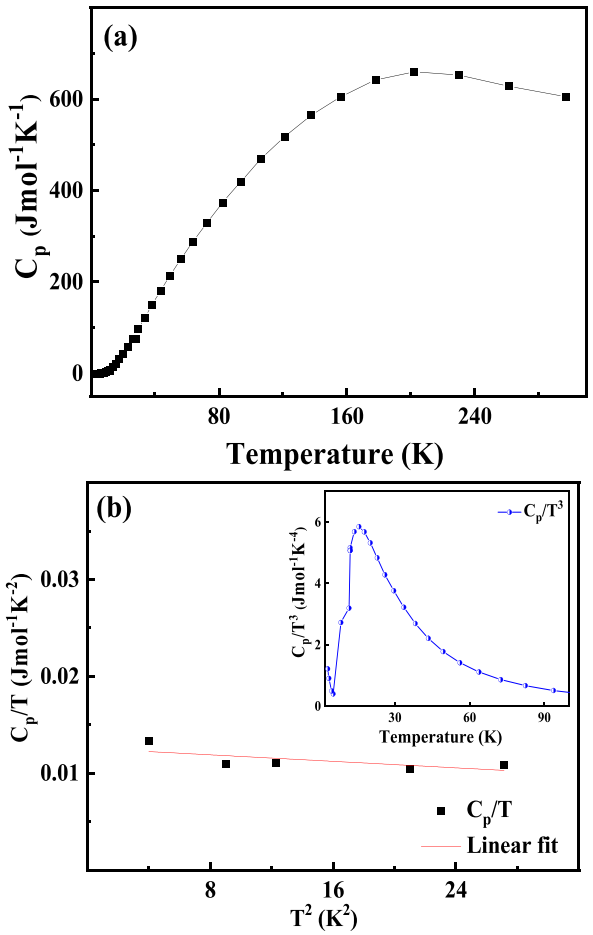

Fig. 10. (a) Temperature dependence of the specific heat capacity (C_p) of $Ba_8Cu_{1.0}Ni_{2.5}Ga_{10}Si_{33.5}$ single crystal clathrate and (b) Low temperature part as C_p/T vs T^2. Electronic contribution calculated by linear fit. Inset of (b) shows C_p/T^3 vs T. The maxima around 15K is indicative of Einstein contribution.

4. Conclusions

In summary, Single crystals of type-I clathrate, $Ba_8Cu_{1.0}Ni_{2.5}Ga_{10}Si_{33.5}$ were synthesized by flux method. PXRD confirmed the phase purity, and a satisfactory refinement model was obtained. The refined composition is in considerable agreement with the starting nominal composition and also matches well with the EDX and XPS data. The presence of strong band around 514 cm^{-1} in the Raman spectrum pointed towards weak framework interactions. Magnetic measurements in low field and low-temperature range revealed weak ferromagnetic behavior that was further evident from heat capacity measurements also. The effective magnetic moment calculated using Curie-Weiss law is 3.87 μ_B. The magnetic hysteresis loop showed spontaneous magnetization at low temperatures. The carrier concentration and carrier mobility of the crystal was found to be 1.8×10^{20} cm^{-3} and 87.7 $cm^2V^{-1}s^{-1}$, respectively.

CRediT authorship contribution statement

Pooja Rawat: Writing – original draft, Visualization, Methodology, Investigation, Funding acquisition, Formal analysis, Data curation, Conceptualization. **Aanchal Sethi:** Methodology, Investigation, Formal analysis, Data curation. **Jin Hee Kim:** Methodology, Investigation, Formal analysis, Data curation. **Jong Soo Rhyee:** Writing – review & editing, Supervision, Resources, Project administration, Investigation, Funding acquisition, Formal analysis, Data curation, Conceptualization.

Declaration of competing interest

The authors declare that they have no known competing financial interests or personal relationships that could have appeared to influence the work reported in this paper.

Acknowledgments

This work was supported by the National Research Foundation of Korea (NRF) funded by the Ministry of Education, Science and Technology (NRF-2019H1D3A1A01070741, RS-2023-00247622, NRF-2021R1A4A3029839).

References

[1] Y. Dong, P. Chai, M. Beekman, X. Zeng, T.M. Tritt, G.S. Nolas, Precursor routes to complex ternary intermetallics: single-crystal and microcrystalline preparation of clathrate-I $Na_8Al_8Si_{38}$ from NaSi + NaAlSi, Inorg. Chem. 54 (2015) 5316–5321.
[2] S. Stefanoski, G.S. Nolas, Synthesis and structural characterization of single-crystal $K_{7.5}Si_{46}$ and $K_{17.8}Si_{136}$ clathrates, Cryst. Growth Des. 11 (2011) 4533–4537.
[3] K. Ghosh, A. Ovchinnikov, M. Baitinger, M. Krnel, U. Burkhardt, Y. Grin, S. Bobev, Lithium metal atoms fill vacancies in the germanium network of a type-I clathrate: synthesis and structural characterization of $Ba_8Li_5Ge_{41}$, Dalton Trans. 52 (2023) 10310–10322.
[4] S. Iwasaki, H. Morito, T. Komine, K. Morita, T. Shibuya, J. Nishii, M. Fujioka, A novel technique for controlling anisotropic ion diffusion: bulk single-crystalline metallic silicon clathrate, Adv. Mater. 34 (2022) 2106754.
[5] J.S. Kasper, P. Hangenuller, M. Pochard, C. Cross, Clathrate structure of silicon Na_8Si_{46} and Na_xSi_{136} (x < 11), Science 150 (1965) 1713–1714.
[6] J. Wang, J.-A. Dolyniuk, K. Kovnir, Unconventional clathrates with transition metal phosphorus frameworks, Acc. Chem. Res. 51 (2018) 31–39.
[7] S. Yamanaka, Silicon clathrates and carbon analogs: high pressure synthesis, structure, and superconductivity, Dalton Trans. 39 (2010) 1901–1915.
[8] K. Suekuni, M.A. Avila, K. Umeo, H. Fukuoka, S. Yamanaka, T. Nakagawa, T. Takabatake, Simultaneous structure and carrier tuning of dimorphic clathrate $Ba_8Ga_{16}Sn_{30}$, Phys. Rev. B 77 (2008) 235119.
[9] H. Anno, M. Hokazono, R. Shirataki, Y. Nagami, Crystallographic, thermoelectric, and mechanical properties of polycrystalline type-I $Ba_8Al_{16}Si_{30}$-based clathrates, J. Mater. Sci. 48 (2013) 2846–2854.
[10] M. Christensen, S. Johnsen, B.B. Iversen, Thermoelectric clathrates of type I, Dalton Trans. 39 (2010) 978–992.
[11] M. Falmbigl, F. Kneidinger, M. Chen, A. Grytsiv, H. Michor, E. Royanian, E. Bauer, H. Effenberger, R. Podloucky, P. Rogl, Cage-forming compounds in the Ba−Rh−Ge system: from thermoelectrics to superconductivity, Inorg. Chem. 52 (2013) 931–943.
[12] M. Beekman, M. Baitinger, H. Borrmann, W. Schnelle, K. Meier, G.S. Nolas, Y. Grin, Preparation and crystal growth of $Na_{24}Si_{136}$, J. Am. Chem. Soc. 131 (2009) 9642–9643.
[13] W. Jung, J. Lörincz, R. Ramlau, H. Borrmann, Y. Prots, F. Haarmann, W. Schnelle, U. Burkhardt, M. Baitinger, Y. Grin, $K_7B_7Si_{39}$, a borosilicide with the clathrate I structure, Angew. Chem. 46 (2007) 6725–6728.
[14] C.L. Condron, R. Porter, T. Guo, S.M. Kauzlarich, Crystal structures, Raman spectroscopy, and magnetic properties of $Ba_{7.5}Al_{13}Si_{29}$ and $Eu_{0.27}Ba_{7.22}Al_{13}Si_{29}$, Inorg. Chem. 44 (2005) 9185–9191.
[15] B.C. Sales, B.C. Chakoumakos, R. Jin, J.R. Thompson, D. Mandrus, Structural, magnetic, thermal, and transport properties of $X_8Ga_{16}Ge_{30}$ (X= Eu, Sr, Ba) single crystals, Phys. Rev. B 63 (2001) 245113.
[16] B.H. Toby, R.B.V. Dreele, GSAS-II: the genesis of a modern open-source allpurpose crystallography software package, J. Appl. Crystallogr. 46 (2013) 544–549.
[17] G. Cordier, P. Woll, New ternary intermetallic compounds with clathrate structure: $Ba_8(T,Si)_6Si_{40}$ and $Ba_6(T,Ge)_6Ge_{40}$ with T = Ni , Pd , Pt , Cu , Ag , Au, J. Less Common. Met. 169 (1991) 291–302.
[18] S. Johnsen, A. Bentien, G.K.H. Madsen, M. Nygren, B.B. Iversen, Crystal structure and transport properties of nickel containing germanium clathrates, Phys. Rev. B 76 (2007) 245126.
[19] K. Wei, A.R. Khabibullin, D. Hobbis, W. Wong-Ng, T. Chang, S.G. Wang, G.S. Nolas, Synthesis, structure, and electrical properties of the single crystal $Ba_8Cu_{16}As_{30}$, Inorg. Chem. 57 (2018) 9327–9334.
[20] C.L. Condron, R. Porter, T. Guo, S.M. Kauzlarich, Crystal structures, Raman spectroscopy, and magnetic properties of $Ba_{7.5}Al_{13}Si_{29}$ and $Eu_{0.27}Ba_{7.22}Al_{13}Si_{29}$, Inorg. Chem. 44 (2005) 9185–9191.
[21] H. Shimizu, T. Kume, T. Kuroda, S. Sasaki, H. Fukuoka, S. Yamanaka, High-pressure Raman study on two modifications of $BaAl_2Si_2$, Phys. Rev. B 68 (2003) 212102.
[22] R. Zhao, S. Bobev, L. Krishna, T. Yang, J.M. Weller, H. Jing, C.K. Chan, Anodes for lithium-ion batteries based on type I silicon clathrate $Ba_8Al_{16}Si_{30}$ - role of processing on surface properties and electrochemical behavior, ACS Appl. Mater. Interfaces 9 (2017) 41246–41257.
[23] T.L. Barr, An XPS study of Si as it occurs in adsorbents, catalysts, and thin films, Appl. Surf. Sci. 15 (1983) 1–35.
[24] D.C. Li, Y.H. Quan, D.H. Ren, S.K. Deng, XPS study and first-principles calculations of the structural and electronic properties of type-VIII clathrates $Ba_8Ga_{16-x}Cu_xSn_{30}$, Adv. Mater. Res. 1058 (2014) 97–101.

[25] W. Shon, J.S. Rhyee, Y. Jin, S.J. Kim, Magnetic polaron and unconventional magnetotransport properties of the single-crystalline compound $EuBiTe_3$, Phys. Rev. B 100 (2019) 024433.
[26] J. Wang, J.-A. Dolyniuk, E.H. Krenkel, J.L. Niedziela, et al., Clathrate $BaNi_2P_4$: an interplay of heat and charge transport due to strong host–guest interactions, Chem. Mater. 32 (2020) 7932–7940.
[27] Y. Li, W. Gou, J. Chi, J.H. Ross Jr., Ferromagnetism and Metamagnetism in Copper-Doped Germanium Clathrate, 2003 arXiv:cond-mat/0305369.
[28] V.V. Novikov, K.S. Pilipenko, A.V. Matovnikov, N.V. Mitroshenkov, M.S. Likhanov, A.S. Tyablikov, A.V. Shevelkov, Effect of the cation sublattice composition of tin based type-I clathrates on their low-temperature thermal properties, Dalton Trans. 47 (2018) 11219.
[29] K. Kovnir, U. Stockert, S. Budnyk, Y. Prots, M. Baitinger, S. Paschen, A.V. Shevelkov, Yuri Grin, Introducing a magnetic guest to a tetrel-free clathrate: synthesis, structure, and properties of $Eu_xBa_{8-x}Cu_{16}P_{30}$ ($0 \leq x \leq 1.5$), Inorg. Chem. 50 (2011) 10387–10396.
[30] M.A. Avila, K. Suekuni, K. Umeo, H. Fukuoka, S. Yamanaka, T. Takabatake, Glasslike versus crystalline thermal conductivity in carrier-tuned $Ba_8Ga_{16}X_{30}$ clathrates (X=Ge, Sn), Phys. Rev. B 74 (2006) 125109.
[31] C. Candolfi, U. Aydemir, A. Ormeci, M. Baitinger, N. Oeschler, F. Steglich, Yu Grin, Low-temperature magnetic, galvanomagnetic, and thermoelectric properties of the type-I clathrates $Ba_8Ni_xSi_{46-x}$, Phys. Rev. B 83 (2011) 205102.
[32] U. Aydemir, C. Candolfi, H. Borrmann, M. Baitinger, A. Ormeci, W. Carrillo-Cabrera, C. Chubilleau, B. Lenoir, A. Dauscher, N. Oeschler, F. Steglich, Y. Grin, Crystal structure and transport properties of $Ba_8Ge_{43}\square_3^{\dagger}$, Dalton Trans. 39 (2010) 1078–1088.